High-Efficiency Bidirectional Three-Phase LCC Resonant Converter With a Wide Load Range

Suk-Ho Ahn, *Member, IEEE*, Sung-Roc Jang, *Member, IEEE*, and Hong-Je Ryoo, *Member, IEEE*

***Abstract*—This paper details the design and implementation of an efficient 4-kW bidirectional converter with a wide load range, based on a three-phase LCC resonant converter operated in a continuous conduction model, which has a number of advantages pertaining to a bidirectional power supply. The voltage boost-up function yields a high voltage gain without increasing the transformer turn ratio. The high switching frequency, which is achievable by using the soft-switching condition and multiphase operation, decreases the output ripple and helps minimize the size of the output filter, as the requirement for a filter changes after the power flow. Moreover, this reduction in the size of the filters yields economic advantages. In addition, because of the synchronous rectifier operation employed during switching, the conduction loss in the rectifier diode of the proposed converter is low. The direction of the output power can be changed easily, using phase control. The implemented power converter is connected to a 320-V rated generator on one side and 28-V lead-acid batteries on the other side. The functionality of the proposed converter is verified in experiments. We confirmed the high performance of the developed converter in terms of efficiency (92.2%), operable load range (0–12.5 A in step-up, and 0–142 A in step-down), and voltage ripple (0.05%).**

***Index Terms*—Bidirectional dc–dc converter, LCC resonant converter, three-phase resonant converter.**

I. Introduction

BIDIRECTIONAL dc–dc converters are widely used in various battery charging and discharging applications, such as renewable energy systems, ESS, UPS, and EV power converters. In general, these applications require high power density, high efficiency, and high reliability for bidirectional dc–dc converters and generally require isolation for safety.

Manuscript received September 25, 2017; revised December 21, 2017 and February 25, 2018; accepted March 4, 2018. Date of publication March 11, 2018; date of current version November 19, 2018. This work was supported in part by the Korea Electrotechnology Research Institute Primary Research Program through the National Research Council of Science and Technology funded by the Ministry of Science, ICT, and Future Planning (MSIP) under Grant 18-12-N0101-28 and in part by the National Research Foundation of Korea funded by the Korea Government (MSIP) under Grant NRF-2017R1A2B 3004855. Recommended for publication by Associate Editor A. Safaee. *(Corresponding author: Hong-Je Ryoo.)*

S.-H. Ahn is with the Accelerator Engineering Team, Pohang Accelerator Laboratory, Pohang 37673, South Korea (e-mail:

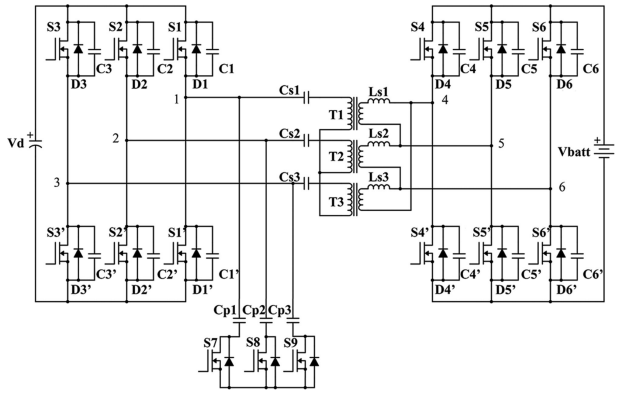

Fig. 1. Schematic of the proposed bidirectional three-phase LCC resonant converter.

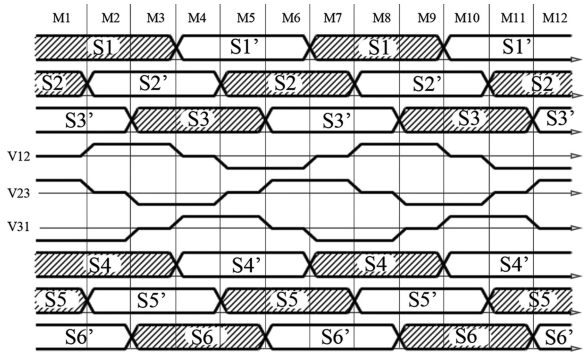

Fig. 2. Switching sequence for the step-down operation of the converter.

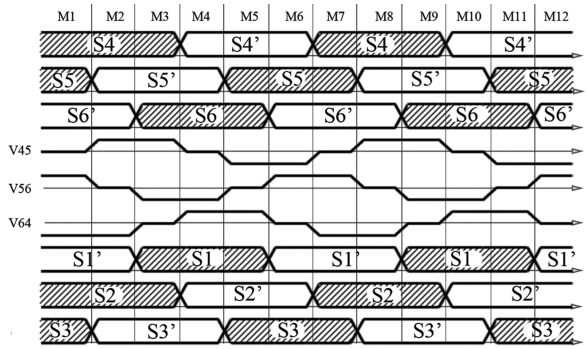

Fig. 3. Switching sequence for the step-up operation of the converter.

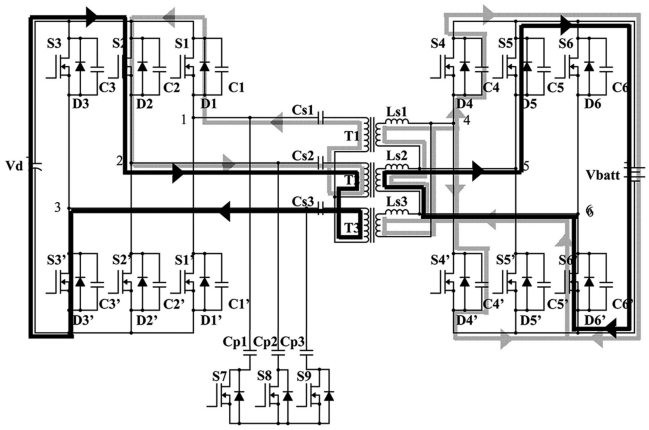

Fig. 4. Operation diagram for analysis of mode 1 of the step-down state.

parallel resonance capacitor only during the step-up operation to compensate for the voltage transfer ratio. In addition, the filter capacitance must be inevitably increased to minimize the voltage ripples at the low voltage part, resulting in a low power density. However, the bidirectional converter based on the proposed LCC resonant converter can achieve a high-power density by minimizing the filter capacitance required in the multiphase operation.

Moreover, the proposed converter can reduce the conduction loss of rectifier diodes by operating the other switches (step-down and step-up) as synchronous rectifiers in the step-up and step-down mode. Another advantage is that the direction of output power can be easily switched through phase control. This paper explains in detail the implementation of the bidirectional three-phase LCC resonant converter and the principle of the operation of the proposed converter, focusing on the efficiency, load range, ripples, and step load response.

II. Operational Principles of the Proposed Converter

The proposed converter, which is shown in Fig. 1, is composed of twelve MOSFETs, three series resonant capacitors, three series resonant inductors, and three additional parallel resonant capacitors. The three additional parallel resonant capacitors are only operated in the step-up mode, to increase the voltage gain from the voltage boost function. Each inverter leg is operated as an LCC resonant converter in the CCM.

Figs. 2 and 3 show the switching sequences for the step-up and step-down operation state, respectively. In this section, operations of the converter in modes 1 and 2 of both the step-down state and the step-up state are explained. The other mode of the converter operation is similar to the explained mode. In the step-down mode, the switches in the step-up leg (S4, S5, S6, S4', S5', S6') are synchronized and operated with the switches in the step-down leg (S1, S2, S3, S1', S2', S3') as a synchronous rectifier, to decrease conduction loss in the rectifier diode. In the step-up mode, switches S7–S9 are turned ON to increase the value of the parallel resonant capacitor, for higher voltage gain from the voltage boost-up function. The switches in the step-down leg are also operated with the switches in the step-up leg switches, as a synchronous rectifier. However, in this mode of operation, the synchronous rectifier has a 120-degree phase shift. With this switching sequence, the direction of the output is changed. Detailed descriptions and principles of operation for each state are discussed below.

Step-down mode 1: The operation diagram for this mode is shown in Fig. 4. The black line depicts the power flow direction, and the grey line expresses the direction of the free-wheeling current. In this mode, switches S2 and S3' are turned ON, and the input current flows through these switches, the series resonant capacitors Cs2, Cs3, and the series resonant inductor Ls2. When the load current flows through D5 and D6', switches S5 and S6' are turned ON as synchronous rectifiers, to decrease conduction loss in the rectifier diode. At the beginning of this mode, the

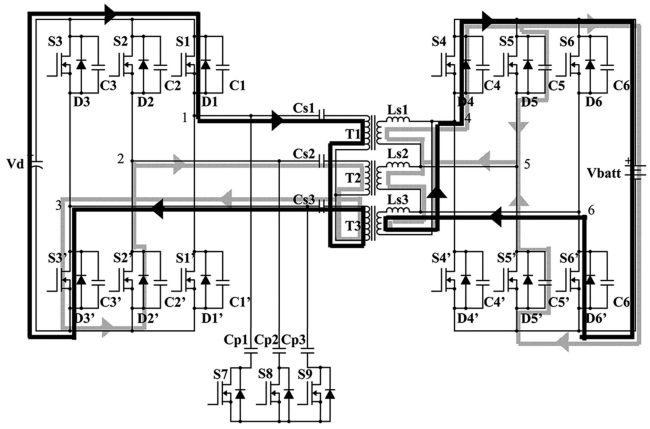

Fig. 5. Operation diagram for analysis of mode 2 of the step-down state.

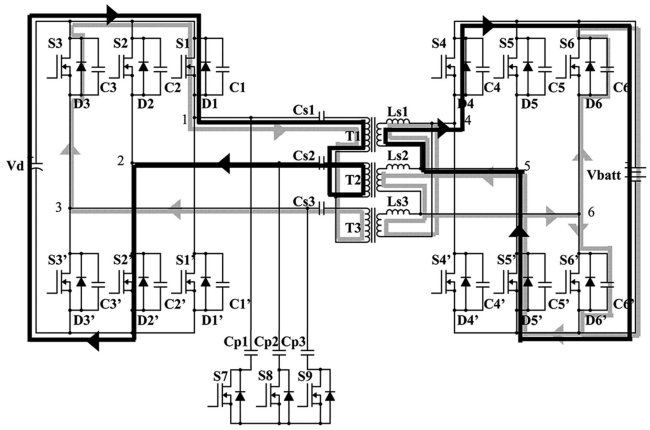

Fig. 6. Operation diagram for analysis of mode 3 of the step-down state.

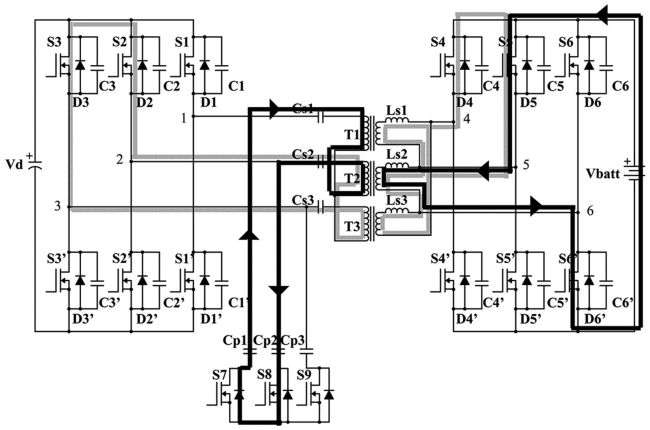

Fig. 7. Operation diagram for analysis of mode 1-1 of the step-up state.

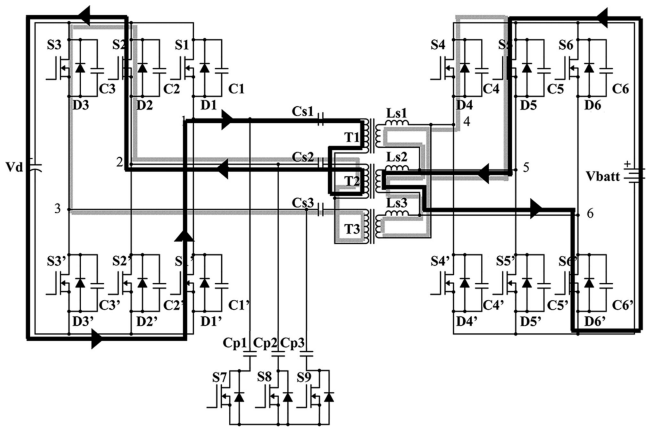

Fig. 8. Operation diagram for analysis of mode 1-2 of the step-up state.

free-wheeling current flows through the lossless snubber capacitor C1, S2, and the resonant tank. After C1 is fully discharged, the free-wheeling current flows through the antiparallel diode D1 of switch S1.

Step-down mode 2: After switch S2 is turned OFF, the input current begins to flow through switch S1. The voltage across switch S2 slowly increases, as a result of charging from the lossless snubber capacitor C2. This operation helps to decrease the turn-OFF loss of the switch. Prior to the beginning of this mode, the voltage and current across switch S1 are almost zero, as a result of the free-wheeling current from mode 1. Thus, switch S1 is turned ON in the zero voltage zero current (ZVZC) condition. The input current flows through switches S1 and S3', the series resonant capacitors Cs1, Cs3, and the series resonant inductor Ls3. In addition, at the beginning of this mode, the free-wheeling current flows through the lossless snubber capacitor C2', S3', and the resonant tank. After C2' is fully discharged, the free-wheeling current flows through the antiparallel diode D2' of switch S2'. When the load current flows through D4 and D6', switches S4 and S6' are turned ON as synchronous rectifiers. The operation diagram for this mode is shown in Fig. 5.

As mentioned above, the switches are turned ON under the ZVZC condition and are turned OFF with low turn-OFF loss because of the lossless snubber capacitors. In the step-down operation, the switches in the step-up side are operated as synchronous rectifiers. Because of this operation, the proposed converter has a high efficiency.

In the step-up mode, switches S7–S9 are always turned ON, to connect to the additional parallel resonant capacitors (Cp1–Cp3). Hence, these switches can be replaced by a relay. The additional parallel resonant capacitors help improve the voltage boost-up function.

Step-up mode 1: The operation diagrams for this mode are shown in Figs. 7 and 8. During this mode, switches S5 and S6' are turned ON, and the input current flows through these switches and the series resonant inductor Ls2. The free-wheeling current flows through the lossless snubber capacitor C4, S5, and the resonant tank. After C4 is fully discharged, the free-wheeling current flows through the antiparallel diode D4 of switch S4.

In the 1-1 mode shown in Fig. 7, the resonant current flows through the parallel resonant capacitors Cp1 and Cp2. The resonant current rises rapidly, as it is influenced by the parallel resonant capacitor, which has a relatively small capacitance. The energy stored in the resonant inductor increases, due to the rise in the resonant current. After charging, the voltage across the parallel resonant capacitors Cp1 and Cp2 is clamped to the output voltage. Current flows through switches S2 and S3' to the load, as shown in Fig. 8.

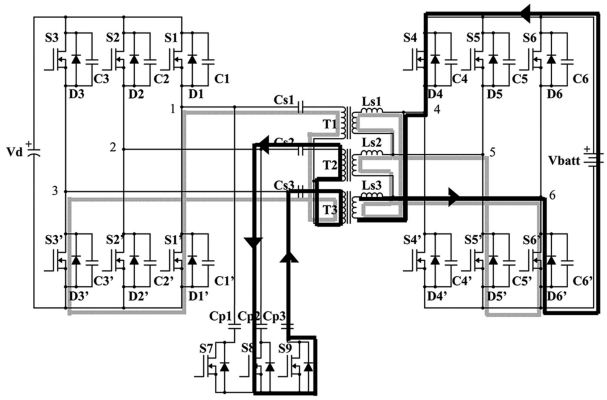

Fig. 9. Operation diagram for analysis of mode 2-1 of the step-up state.

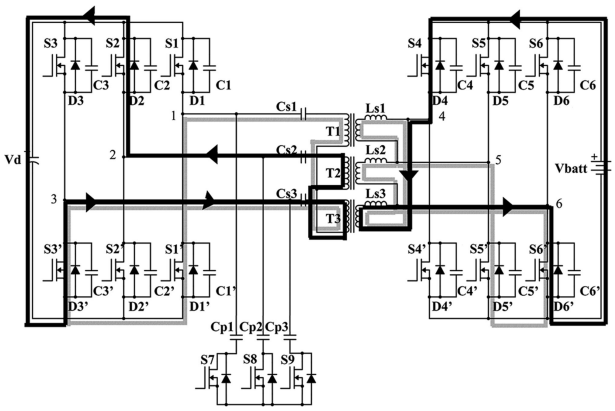

Fig. 10. Operation diagram for analysis of mode 2-2 of the step-up state.

Step-up mode 2: This mode begins after switch S5 is turned OFF and the input current starts to flow through switch S4. The voltage across switch S5 increases slowly, as a result of charging from the lossless snubber capacitor C5. This operation helps to decrease turn-OFF loss in the switch. Prior to the beginning of this mode, the voltage and current across switch S4 are almost zero, as a result of the free-wheeling current. Thus, S4 is turned ON under the ZVZC condition. The input current flows through S4 and S6', and free-wheeling current flows through S5' and S6'. The influence of the parallel resonant capacitors (Cp2, Cp3) on the resonant current in this mode is shown in Fig. 9. The load current flows through switches S2 and S3', as shown in Fig. 10.

III. Implementation of a 4-kW Bidirectional Converter

A prototype of the proposed 4-kW converter was built, for verifying the functionality of the device as a bidirectional power supply. Table I shows the required specifications for the step-down operation, and Table II shows the required specifications for the step-up operation of the prototype. These specifications were used in the implementation of the prototype. The 4-kW bidirectional power supply prototype is connected to a generator as the step-up side load and lead-acid batteries as the step-down side load. The rated voltage of the load batteries is 28 V, and the voltage of the load generator is 320 V.

TABLE I
Specifications for the Step-Down Operation of the Converter

Input voltage	320 V ± 16 V
Transient voltage (during a 3-second period after switching)	260–360 V
Maximum input current	16 A (<5 kW)
Output voltage at the steady state (less than 5% load variation)	28 V ± 1.4 V
Controllable output current and limit voltage range	0–142 A at 18–32 V
Output voltage ripple	Less than 2 Vpk
Rated output power	>4 kW (28 V, 143 A)
Instantaneous maximum output power (during a 1.5-second period after switching)	5 kW (179 A)
Efficiency at rated operation	>90%
Output voltage variation range for 100% step load response	24–29.5 V
Settling time for 100% step load response	<3 s

TABLE II
Specifications for the Step-Up Operation of the Converter

Input voltage	24 V ± 2 V
Transient voltage (during a 3-second period after switching)	21–32 V
Maximum input current	175 A (<5 kW)
Output voltage at the steady state (less than 5% load variation)	320 V ± 9.6 V
Controllable output current and limit voltage range	0–16 A at 256–320 V
Output voltage ripple	Less than 5 Vpk
Rated output power	>4 kW (320 V, 13 A)
Instantaneous maximum output power (during a 1.5-second period after switching)	5 kW (16 A)
Efficiency at rated operation	>90%
Output voltage variation range for 100% step load response	280–350 V
Settling time for 100% step load response	<3 s

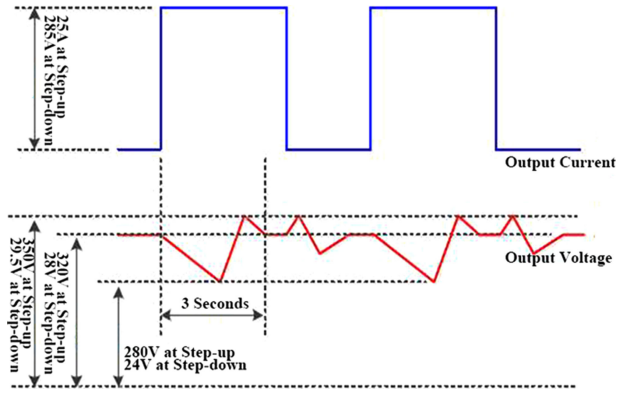

Fig. 11. Required transient response for the step-up/step-down operation of the converter.

The power supply is required to operate with a wide output current (0–16 A during the step-up operation, and 0–142 A during the step-down operation), achieve low ripple (2 V peak-to-peak in the step-up operation, 5 V peak-to-peak in the step-down operation), and high efficiency (>90%). The specification for the step load response of the prototype bidirectional power supply is shown in Fig. 11. A stable output is required from the power supply, within 3 seconds of switching, against a 100% step load.

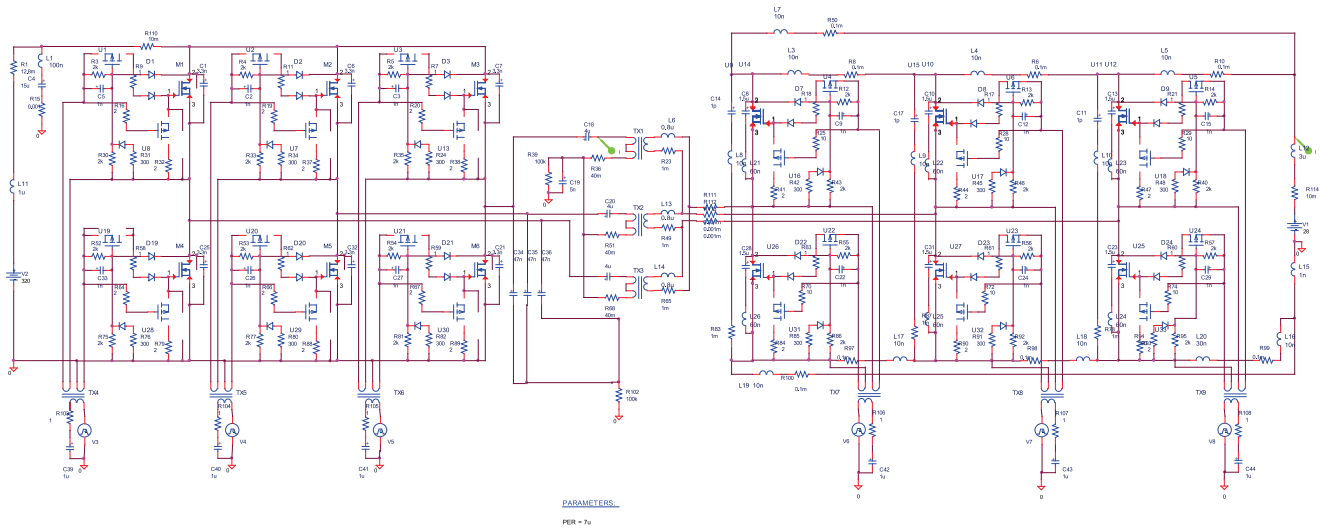

Fig. 12. PSpice model of the bidirectional three-phase LCC resonant converter.

TABLE III
DESIGNED PARAMETERS OF THE CONVERTER

Component	Value
Series resonant capacitors (Cs1–Cs3)	4 μF
HV snubber capacitors (C1–C3')/parallel resonant capacitors	3.3 nF
LV snubber capacitors (C4–C6')/parallel resonant capacitors	1.5 μF
Transformer turn ratio	4:22
Resonant inductor (leakage inductance)	0.8 μH
Additional resonant capacitors (Cp1–Cp3)	47 nF
HV filter capacitor	15 μF
LV filter capacitor	150 μF

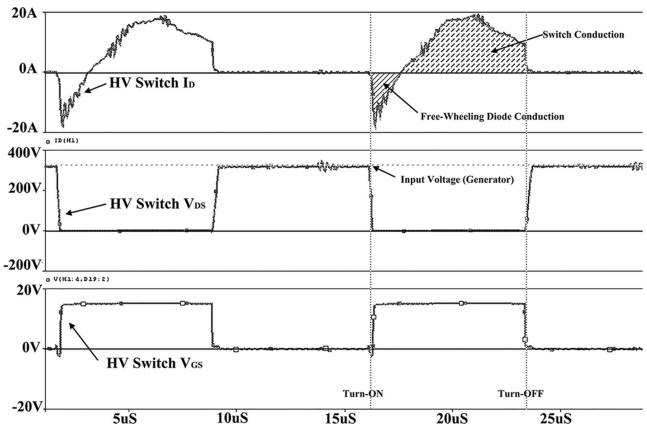

Fig. 13. Simulation waveforms for the step-down operation mode with a 4-kW rated load.

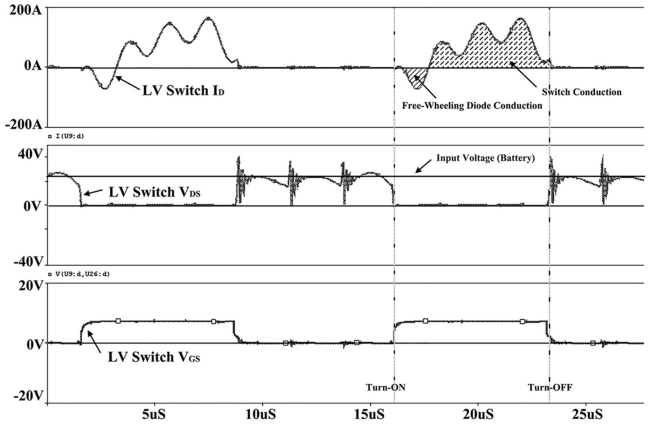

Fig. 14. Simulation waveforms for the step-up operation mode with a 4-kW rated load.

The size and weight of the implemented 4-kW bidirectional power supply are less than 450 mm $\times$ 500 mm $\times$ 250 mm and 55 kg. The schematic of the power supply, which is used as a PSpice simulation model, is shown in Fig. 12. The design parameters of the power supply are shown in Table III.

Figs. 13 and 14 show the simulation result waveforms for the voltages at both ends of the switch, switch current, and gate signals under the rated load condition of 4 kW. As with the general characteristics of the LCC resonant converter, the designed converter naturally performs soft switching at zero voltage and zero current conditions as current flows through the switch by resonance after the turn-ON gate signal is applied and the current flows through the parallel diodes in the switch at the time of turn ON. Furthermore, at the time of turn OFF, the voltages at both ends of the switch are slowly increased by the lossless snubber capacitor (HV switch; 3.3 nF; LV switch 1.5 μF) connected in parallel in the switch, thus reducing the turn-OFF loss.

Fig. 15 shows the control block diagram of the designed power supply. The error signal is output through the PI controller for the real voltage/current and reference voltage current measured through the voltage divider and the direct-current current transformer. If this signal is input through the frequency modulation IC, a frequency to control the output is formed. This frequency signals have the range of 420 kHz to 1.8 MHz, which is six times larger than the actual switching frequency. This signal is input to the clock of a 3-bit Johnson-Counter and outputs a switching frequency signal (70–300 kHz) that has a phase difference of 120°. The switching frequency signals are divided

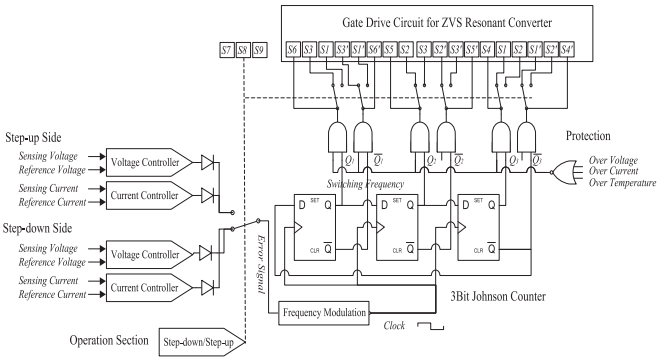

Fig. 15. Control block diagram of the bidirectional three-phase LCC resonant converter.

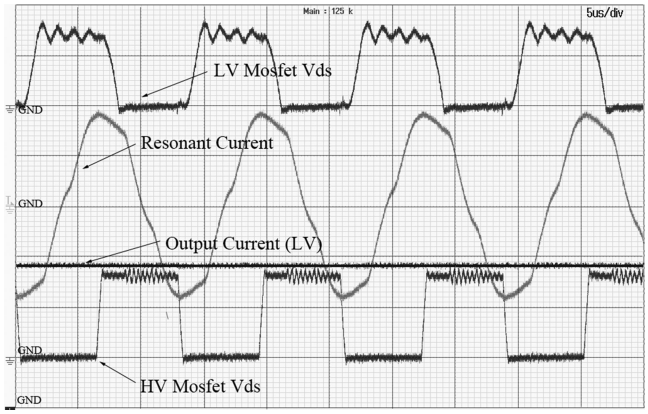

Fig. 16. Experimental waveforms of the power supply during the step-down operation with a 4-kW load [time scale: 5 μs/div.; resonant current, 10 A/div.; HV MOSFET (step-up) $V_{\rm ds}$, 200 V/div.; LV MOSFET (step-down) $V_{\rm ds}$, 20 V/div.; output current (LV), 50 A/div.].

through the analog control switch, and the gate signals with the forms of Figs. 2 and 3 are input to the gate driver circuit of each switch. As in [31]–[35], the designed gate drive circuit of the power system operates the LCC resonant converter using a gate driver with zero voltage detection feature, and turn ON is only performed when the current flows through the parallel diode of the switch at the time of operating the synchronous rectifier.

IV. Experimental Results

In this section, results of experiments performed using the 4-kW bidirectional power supply based on the proposed converter, to verify its functionality and that it satisfies the operational requirements detailed in Tables II and III, are discussed.

Fig. 16 shows experimental waveforms of voltage and current during the step-down operation with a 4-kW rated load resistor. As shown in Fig. 16, the peak of the resonant current is about 18 A, and the switching frequency is 70 kHz. During the step-down operation, the MOSFET switches on the step-up side are also operated as synchronous rectifiers, to decrease their conduction loss. Because of this operation, the total measured efficiency of the power supply is 92.2%. Fig. 17 shows experimental current and voltage waveforms during the step-down operation with no load. The peak of the resonant current is about 3 A, and the switching frequency is 298 kHz. Thus, we verified that the

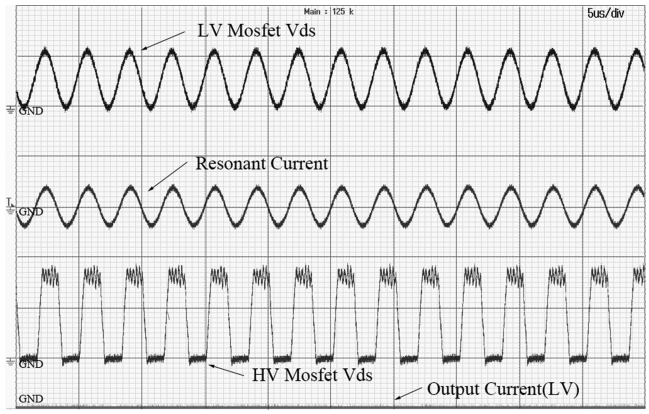

Fig. 17. Experimental waveforms of the power supply during the step-down operation with no load [time scale: 5 μs/div.; resonant current, 20 A/div.; HV MOSFET (step-up) $V_{\rm ds}$, 200 V/div.; LV MOSFET (step-down) $V_{\rm ds}$, 20 V/div.; output current (LV), 50 A/div.].

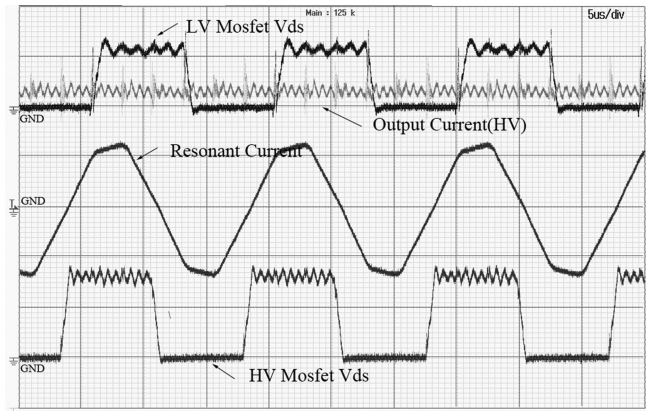

Fig. 18. Experimental waveforms of the power supply during the step-up operation with a 4-kW load [time scale: 5 μs/div.; resonant current, 20 A/div.; HV MOSFET (step-up) $V_{\rm ds}$, 200 V/div.; LV MOSFET (step-down) $V_{\rm ds}$, 20 V/div.; output current (HV), 2 A/div.].

implemented bidirectional power supply can be operated with high efficiency in the step-down mode, and with a wide range of loads, from no-load to a 4-kW rated load.

Figs. 18 and 19 show experimental waveforms during the step-up operation. As shown in Fig. 18, the peak of the resonant current, measured at the step-down side of the transformer, is 21 A, and the switching frequency is 68 kHz.

At the beginning of the resonance condition, the current increases rapidly because of the additional parallel resonant capacitor. Hence, the resonant current has a low crest factor, which decreases the conduction loss. Fig. 19 shows experimental waveforms during the step-up operation under the no-load condition. In this case, the peak of the resonant current, measured at the step-down side of the transformer, is 10 A, and the switching frequency is 203 kHz. We also verified that the power supply can be operated with a wide load range in the step-up mode.

Figs. 20 and 21 show the results of output voltage ripple measurements performed during the step-down and step-up operation. During the step-up operation with a rated resistor load, the measured output voltage ripple is 0.5 V peak-to-peak. In the step-down operation with a rated resistor load, the measured

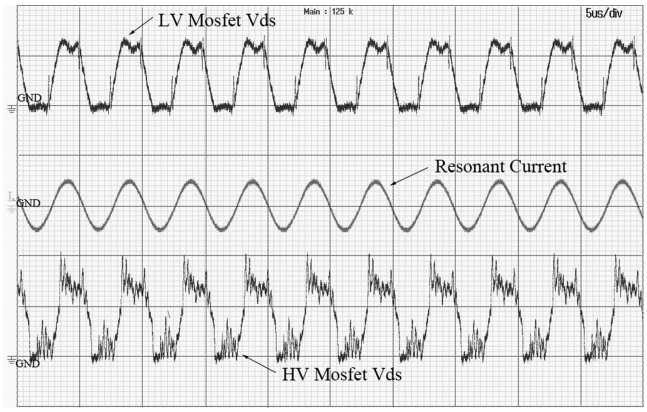

Fig. 19. Experimental waveforms of the power supply during the step-up operation with no load [time scale: 5 μs/div.; resonant current, 20 A/div.; HV MOSFET (step-up) $V_{\rm ds}$, 200 V/div.; LV MOSFET (step-down) $V_{\rm ds}$, 20 V/div.].

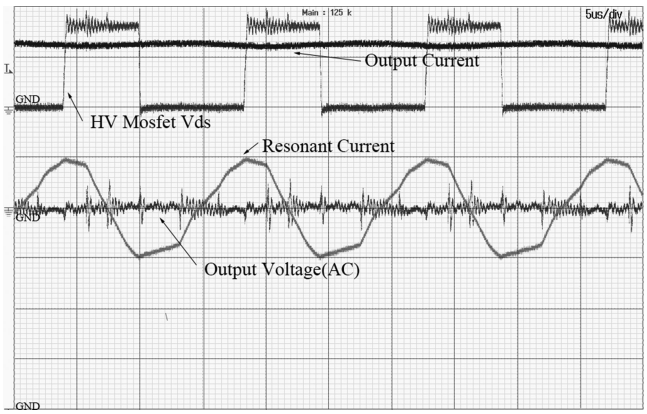

Fig. 20. Experimental waveforms of the output voltage ripple during the step-down operation [time scale: 5 μs/div.; resonant current, 20 A/div.; HV MOSFET (step-up) $V_{\rm ds}$, 200 V/div.; output current, 20 A/div.; output voltage (ac), 1 V/div.].

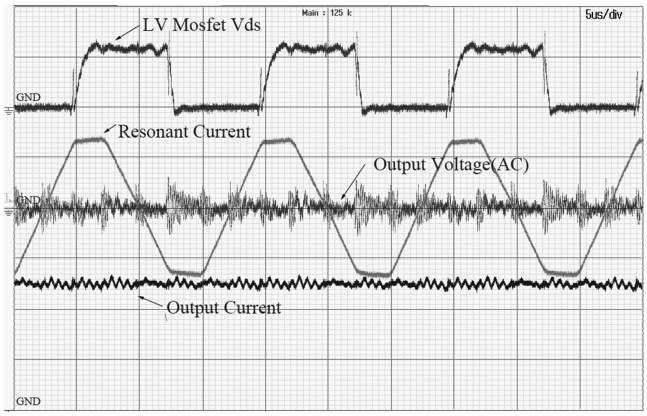

Fig. 21. Experimental waveforms of the output voltage ripple during the step-up operation [time scale: 5 μs/div.; resonant current, 20 A/div.; HV MOSFET (step-up) $V_{\rm ds}$, 200 V/div.; output current, 5 A/div.; output voltage (ac), 2 V/div.].

output voltage ripple is 1 V peak-to-peak. We expect the output voltage ripple to decrease if the power supply is operated with a real load (generator and batteries), instead of the rated resistors used in the detailed experiments, as the implemented bidirectional power supply is designed to reduce ripples through the

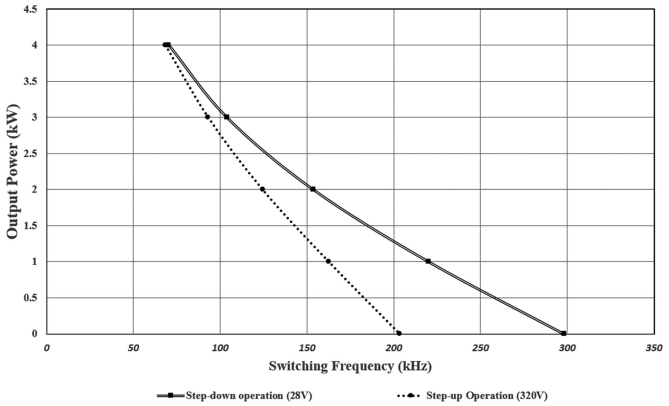

Fig. 22. Measured output power with respect to switching frequency.

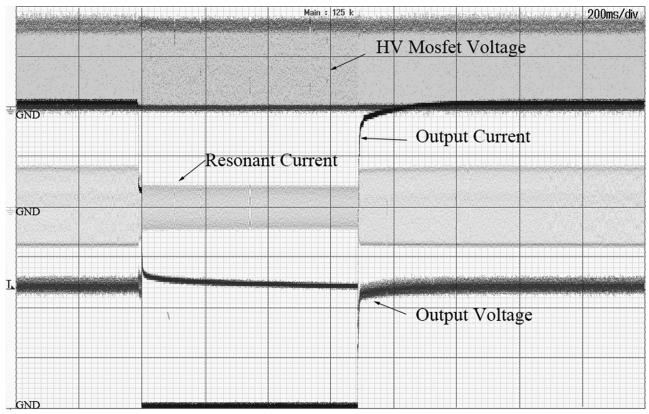

Fig. 23. Experimental waveforms of the step load response during the step-down operation (time scale: 100 ms/div.; resonant current, 20 A/div.; LV MOSFET $V_{\rm ds}$, 20 V/div.; output current, 5 A/div.; output voltage, 100 V/div.).

multiphase operation (three-phase) with a high switching frequency (70–200 kHz), without increasing the number of components in the output filter.

Fig. 22 shows the measured output power with respect to the switching frequency during the step-down operation with a 28 V output and the step-up operation with a 320 V output.

To measure the step load response characteristic of the power supply, the load is suddenly disconnected and reconnected using a circuit breaker, during a 4-kW rated operation. As shown in Fig. 23, which depicts the results of step load response experiments performed in the step-down operation, the power supply can be operated with output voltage fluctuations below 1 V, when the load is rapidly disconnected and reconnected. The measured settling time with a 100% step load is below 10 ms. The response of the output voltage satisfies the system requirements shown in Table II, where voltage fluctuations of less than 9.6 V for a 320 V output are satisfactory. Fig. 24 shows the results of step load response experiments performed during the step-up operation. The power supply can be operated with output voltage fluctuations below 1.4 V, which settle within 10 ms. These characteristics also satisfy the step load response requirements detailed in Table I. We posit that in comparison to the results obtained with the purely resistive load, an improved response

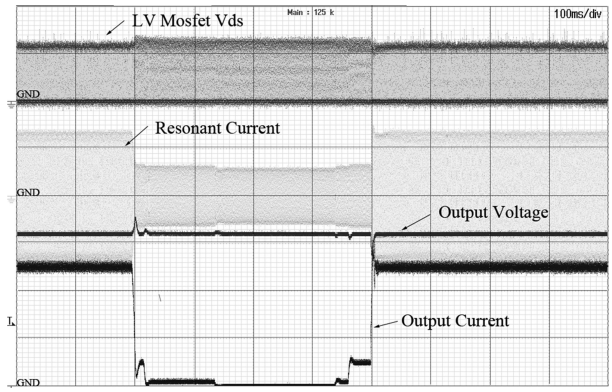

Fig. 24. Experimental waveforms of the step load response during the step-up operation (time scale: 100 ms/div.; resonant current, 20 A/div.; LV MOSFET $V_{\rm ds}$, 20 V/div.; output current, 5 A/div.; output voltage, 100 V/div.).

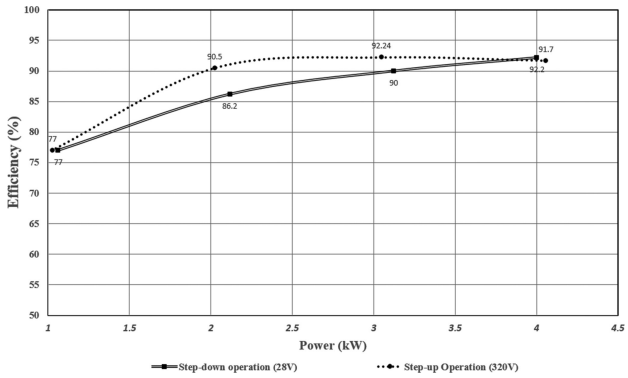

Fig. 25. Result of efficiency measurement.

will be observed with a real load, due to the capacitors of the generator and the batteries.

Finally, Fig. 25 shows the result of efficiency measurement of the implemented bidirectional power supply, during the step-down and step-up operation. From this image, it can be seen that the maximum efficiency measured is 92.2% during the step-down operation with a 28 V output and 91.7% during the step-up operation with a 320 V output. Thus, it has been verified that a bidirectional power supply based on the converter proposed in this paper can be operated with high efficiency. We have also demonstrated that the proposed converter is suitable for use as a bidirectional power supply.

V. Conclusion

In this paper, a bidirectional three-phase LCC resonant converter with high output voltage gain is presented, which is applicable to bidirectional power supplies. The proposed converter has the general advantages of LCC resonant converters operating in the CCM, especially when used as a bidirectional power supply. The voltage boost-up function yields a high voltage gain without increasing the transformer turn ratio. The high switching frequency, resulting from the soft-switching condition and multiphase operation, can decrease the output ripple and help minimize the size of the output filter, as the requirement for a filter changes after the power flow, which yields certain economic advantages. The conduction loss in the rectifier diode of the proposed converter is low due to the synchronous rectifier operation. The direction of the output power can be changed easily through phase control. We demonstrated the high performance of the proposed converter, with respect to a wide operable load range, a low output voltage ripple, and an efficient step response characteristic. The operational principle of the proposed converter was also explained. The design and implementation of a 4-kW bidirectional power supply, based on the proposed converter, was presented. During experiments, one side of the power supply was connected to a 320-V rated generator, and the other side was connected to 28-V rated lead-acid batteries.

Finally, the developed bidirectional power supply was tested with a resistor load. We observed a maximum efficiency of 92.2%, during the step-down operation and 91.7% in the step-up operation, and a controllable load range of 0–28 V, in the step-down operation and 0–320 V in the step-up operation. The output voltage ripple was 1 V in the step-down operation and 1.4 V in the step-up operation. Thus, we verified that the proposed converter topology can be used effectively for a high voltage gain bidirectional power supply.

References

[1] K. Wang, C. Y. Lin, L. Zhu, D. Qu, F. C. Lee, and J. S. Lai, "Bi-directional dc/dc converters for fuel cell systems," in *Proc. IEEE Trans. Power Electron.*, Oct. 1998, pp. 47–51.

[2] F. Z. Peng, H. Li, G.-J. Su, and J. S. Lawler, "A new ZVS bidirectional dc–dc converter for fuel cell and battery application," *IEEE Trans. Power Electron.*, vol. 19, no. 1, pp. 54–65, Jan. 2004.

[3] L. Zhu, "A novel soft-commutating isolated boost full-bridge ZVS PWM dc–dc converter for bidirectional high power applications," *IEEE Trans. Power Electron.*, vol. 21, no. 2, pp. 422–429, Mar. 2006.

[4] D. P. Urciuoli and C. W. Tipton, "Development of a 90 kW bidirectional dc–dc converter for power dense applications," in *Proc. IEEE Appl. Power Electron. Conf.*, 2006, pp. 1375–1378.

[5] J. Lee, J. Jo, S. Choi, and S.-B Han, "A 10-kW SOFC low-voltage battery hybrid power conditioning system for residential use," *IEEE Trans. Energy Convers.*, vol. 21, no. 2, pp. 575–585, Jun. 2006.

[6] M. N. Kheraluwala, R. W. Gascoigne, D. M. Divan, and E. D. Baumann, "Performance characterization of a high-power dual active bridge dc-to-dc converter," *IEEE Trans. Ind. Appl.*, vol. 28, no. 6, pp. 1294–1301, Dec. 1992.

[7] F. Krismer, S. Round, and J. W. Kolar, "Performance optimization of a high current dual active bridge with a wide operating voltage range," in *Proc. IEEE Power Electron. Spec. Conf.*, 2006, pp. 1–7.

[8] F. Krismer and J. W. Kolar, "Accurate small-signal model for the digital control of an automotive bidirectional dual active bridge," *IEEE Trans. Power Electron.*, vol. 24, no. 12, pp. 2756–2768, Dec. 2009.

[9] S. Inoue and H. Akagi, "A bidirectional dc–dc converter for an energy storage system with galvanic isolation," *IEEE Trans. Power Electron.*, vol. 22, no. 6, pp. 2299–2306, Nov. 2007.

[10] F. Krismer and J. W. Kolar, "Accurate power loss model derivation of a high-current dual active bridge converter for an automotive application," *IEEE Trans. Power Electron.*, vol. 57, no. 3, pp. 881–891, Mar. 2010.

[11] C. Leung, S. Dutta, S. Baek, and S. Bhattacharya, "Design considerations of high-voltage and high-frequency three-phase transformer for solid state transformer application," in *Proc. IEEE Energy Convers. Congr. Expo.*, 2010, pp. 1551–1558.

[12] J. Zhang, F. Zhang, X. Xie, D. Jiao, and Z. Qian, "A novel ZVS dc/dc converter for high-power applications," *IEEE Trans. Power Electron.*, vol. 19, no. 2, pp. 420–429, Mar. 2004.

[13] H. Bai and C. Mi, "Eliminate reactive power and increase system efficiency of isolated bidirectional dual-active-bridge dc–dc converter using novel dual-phase-shift control," *IEEE Trans. Power Electron.*, vol. 23, no. 6, pp. 2905–2914, Nov. 2008.

[14] G. G. Oggier, G. O. Garc´ıa, and A. R. Oliva, "Switching control strategy to minimize dual active bridge converter losses," *IEEE Trans. Power Electron.*, vol. 24, no. 7, pp. 1826–1838, Jul. 2009.

[15] G. G. Oggier, G. O. Garc´ıa, and A. R. Oliva, "Modulation strategy to operate the dual active bridge dc–dc converter under soft-switching in the whole operating range," *IEEE Trans. Power Electron.*, vol. 26, no. 4, pp. 1228–1236, Apr. 2011.
[16] B. Zhao, Q. Yu, and W. Sun, "Extended-phase-shift control of isolated bidirectional dc–dc converter for power distribution in microgrid," *IEEE Trans. Power Electron.*, vol. 27, no. 11, pp. 4667–4680, Nov. 2012.
[17] F. Krismer and J. W. Kolar, "Efficiency-optimized high-current dual active bridge converter for automotive applications," *IEEE Trans. Ind. Electron.*, vol. 59, no. 7, pp. 2745–2760, Jul. 2012.
[18] G. Ortiz, J. Biela, D. Bortis, and J. W. Kolar, "1 Megawatt, 20 kHz, isolated, bidirectional 12 kV to 1.2 kV dc–dc converter for renewable energy applications," in *Proc. Int. Power Electron. Conf.*, 2010, pp. 3212–3219.
[19] X. Li and A. K. Bhat, "Analysis and design of high-frequency isolated dual-bridge series resonant dc/dc converter," *IEEE Trans. Power Electron.*, vol. 25, no. 4, pp. 850–862, Apr. 2010.
[20] Y. Du, X. Bian, S. Lukic, B. S. Jacobson, and A. Q. Huang, "A novel wide voltage range bi-directional series resonant converter with clamped capacitor voltage," in *Proc. IEEE Ind. Electron. Soc.*, 2009, pp. 82–87.
[21] G. Pledl, M. Tauer, and D. Buecherl, "Theory of operation, design procedure and simulation of a bidirectional LLC resonant converter for vehicular applications," in *Proc. IEEE Veh. Power Propuls. Conf.*, 2010, pp. 1–5.
[22] T. Jiang, J. Zhang, X. Chen, and Y Wang, "Bidirectional LLC resonant converter for energy storage applications," in *Proc. IEEE Appl. Power Electron. Conf.*, 2013, pp. 1145–1151.
[23] L. Corradini, D. Seltzer, D. Bloomquist, R. Zane, D. Maksimovic, and B. Jacobson, "Minimum current operation of bidirectional dual-bridge series resonant dc/dc converters," *IEEE Trans. Power Electron.*, vol. 27, no. 7, pp. 3266–3276, Jul. 2012.
[24] S. Abe, J. Yamamoto, T. Zaitsu, and T. Ninomiya, "Operating strategy for bi-directional LLC resonant converter with seamless operation," in *Proc. Int. Power Electron. Conf.*, Hiroshima, Japan, 2014, pp. 1179–1184.
[25] W. Chen, P. Rong, and Z. Lu, "Snubberless bidirectional dc–dc converter with new CLLC resonant tank featuring minimized switching loss," *IEEE Trans. Ind. Electron.*, vol. 57, no. 9, pp. 3075–3086, Sep. 2010.
[26] J. Biela, "Optimierung des elektromagnetisch integrierten serien-parallel resonanzkonverters mit eingeprägtem ausgangsstrom," *Ph.D. dissertation*, ETH Zürich, Zürich, Switzerland, 2005.
[27] R. W. De Doncker, D. M. Divan, and M. H. Kheraluwala, "A three phase soft-switched high power density dc-to-dc converter for high power applications," *IEEE Trans. Ind. Appl.*, vol. 27, no. 1, pp. 63–73, Jan./Feb. 1991.
[28] N. Fu-Ming and L. Tzung-Lin, "Implementation of a bidirectional three phase dual-active-bridge dc converter with hybrid modulation for electric vehicle applications," in *Proc. Int. Conf. Intell. Green Build. Smart Grid*, Apr. 2014, pp. 1–4.
[29] H. van Hoek, M. Neubert, A. Kroeber, and R. W. De Doncker, "Comparison of a single-phase and a three-phase dual active bridge with low-voltage, high-current output," in *Proc. Int. Conf. Renewable Energy Res. Appl.*, Nov. 2012, pp. 1–6.
[30] G.-J. Su and L. Tang, "A three-phase bi-directional dc-dc converter for automotive applications," in *Proc. IEEE Ind. Appl. Soc. Annu. Meeting*, Oct. 2008, pp. 1–7.
[31] T. B. Soeiro, J. Mühlethaler, J. Linnér, P. Ranstad, and J. W. Kolar, "Automated design of a high-power high-frequency LCC resonant converter for electrostatic precipitators," *IEEE Trans. Ind. Electron.*, vol. 60, no. 11, pp. 4805–4819, Nov. 2013.
[32] S. H. Ahn, H. J. Ryoo, J. W. Gong, and S. R. Jang, "Low-ripple and high-precision high-voltage dc power supply for pulsed power applications," *IEEE Trans. Plasma Sci.*, vol. 42, no. 10, pp. 3023–3033, Oct. 2014.
[33] S. R. Jang, J. H. Seo, and H. J. Ryoo, "Development of 50-kV 100-kW three-phase resonant converter for 95-GHz gyrotron," *IEEE Trans. Ind. Electron.*, vol. 63, no. 11, pp. 6674–6683, Nov. 2016.
[34] J. W. Gong, H. J. Ryoo, S. H. Ahn, and S. R. Jang, "Design and implementation of a 40-kV, 20-kJ/s capacitor charger for pulsed-power application," *IEEE Trans. Plasma Sci.*, vol. 42, no. 11, pp. 3623–3632, Nov. 2014.
[35] S. R. Jang, C. Yu, and H. J. Ryoo, "Trapezoidal approximation of LCC resonant converter and design of multi-stage capacitor charger for solid-state Marx modulator," in *IEEE Trans. Power Electron.*, vol. 33, no. 5, pp. 3816–3825, May 2018.
[36] A. J. Gilbert, C. M. Bingham, D. A. Stone, and M. P. Foster, "Normalized analysis and design of LCC resonant converters," *IEEE Trans. Power Electron.*, vol. 22, no. 6, pp. 2386–2402, Nov. 2007.
[37] T. B. Soeiro, J. Mühlethaler, J. Linnér, P. Ranstad, and J. W. Kolar, "Automated design of a high-power high-frequency LCC resonant converter for electrostatic precipitators," *IEEE Trans. Ind. Electron.*, vol. 60, no. 11, pp. 4805–4819, Nov. 2013.
[38] M. C. Tsai, "Analysis and implementation of a full-bridge constant-frequency LCC-type parallel resonant converter," *IEE Proc., Electr. Power Appl.*, vol. 141, no. 3, pp. 121–128, May 1994.
[39] H. I. Sewell, M. P. Foster, C. M. Bingham, D. A. Stone, D. Hente, and D. Howe, "Analysis of voltage output LCC resonant converters, including boost mode operation," *IEE Proc., Electr. Power Appl.*, vol. 150, no. 6, pp. 673–679, Nov. 2003.
[40] A. J. Gilbert, D. A. Stone, and C. M. Bingham, "Rapid design of LCC current-output resonant converters with reduced electrical stresses," *Electron. Lett.*, vol. 41, no. 6, pp. 365–366, Mar. 2005.

Suk-Ho Ahn (M'11) received the B.S. degree from Incheon National University, Incheon, South Korea, in 2009, and the Ph.D. degree from the University of Science and Technology, Daejeon, South Korea, in 2015, both in electrical engineering.

In 2016, he was a Postdoctoral Research Fellow with the Korea Electrotechnology Research Institute, Changwon, South Korea. Since 2016, he has been a Staff Scientist with the Department of Accelerator R&D, Pohang Accelerator Laboratory, Pohang, South Korea. His research interests include high-voltage, high-power converter, and solid-state pulsed power modulator.

Sung-Roc Jang (M'11) was born in Daegu, South Korea, in 1983. He received the B.S. degree from Kyungpook National University, Daegu, South Korea, in 2008, and the M.S. and Ph.D. degrees in electrical engineering from the University of Science and Technology, Daejeon, South Korea, in 2011.

Since 2011, he has been with the Korea Electrotechnology Research Institute, Changwon, South Korea, as a Senior Researcher with the Electric Propulsion Research Center. In 2015, he became an Assistant Professor with the Department of Energy Conversion Technology, University of Science and Technology. His current research interests include high-voltage resonant converters and solid-state pulsed power modulators and their industrial applications.

Dr. Jang was a recipient of the Young Scientist Award at the 3rd Euro-Asian Pulsed Power Conference in 2010, and the IEEE Nuclear Plasma Science Society Best Student Paper Award at the IEEE International Pulsed Power Conference in 2011.

Hong-Je Ryoo (M'17) received the B.S., M.S., and Ph.D. degrees in electrical engineering from SungKyunkwan University, Seoul, South Korea, in 1991, 1995, and 2001, respectively.

From 2004 to 2005, he was a Visiting Scholar for his postdoctoral study with the Wisconsin Electric Machines and Power Electronics Consortium, University of Wisconsin-Madison, Madison, WI, USA. During 1996–2015, he was with the Korea Electrotechnology Research Institute, Changwon, South Korea, where he joined the Electric Propulsion Research Division, as a Principal Research Engineer, in 2008, and was a Leader of the Pulsed Power World Class Laboratory. He was a Professor with the Department of Energy Conversion Technology, University of Science and Technology, Daejeon, South Korea. In 2015, he joined the School of Energy Systems Engineering, Chung-Ang University, Seoul, South Korea, where he is currently an Associate Professor. His current research interests include pulsed-power systems and their applications, as well as high-power and high-voltage conversions.

Dr. Ryoo is a Member of the Korean Institute of Power Electronics and the Korean Institute of Electrical Engineers.